Bridging particle deformability and collective response in soft solids

John D. Treado,[1,2,*] Dong Wang,[1,*] Arman Boromand,[1] Michael P. Murrell,[3,4,5] Mark D. Shattuck,[6] and Corey S. O'Hern[1,4,7,2,†]

[1]*Department of Mechanical Engineering & Materials Science, Yale University, New Haven, Connecticut 06520, USA*
[2]*Integrated Graduate Program in Physical and Engineering Biology, Yale University, New Haven, Connecticut 06520, USA*
[3]*Department of Biomedical Engineering, Yale University, New Haven, Connecticut 06520, USA*
[4]*Department of Physics, Yale University, New Haven, Connecticut 06520, USA*
[5]*Systems Biology Institute, Yale University, West Haven, Connecticut 06516, USA*
[6]*Benjamin Levich Institute and Physics Department, The City College of New York, New York, New York 10031, USA*
[7]*Department of Applied Physics, Yale University, New Haven, Connecticut 06520, USA*

(Dated: December 5, 2020)

Soft, amorphous solids such as tissues, foams, and emulsions are composed of deformable particles. However, the effect of single-particle deformability on the collective behavior of soft solids is still poorly understood. We perform numerical simulations of two-dimensional jammed packings of explicitly deformable particles to study the mechanical response of model soft solids. We find that jammed packings of deformable particles with excess shape degrees of freedom possess low-frequency quartic vibrational modes that stabilize the packings even though they possess fewer interparticle contacts than the nominal isostatic value. Adding intra-particle constraints can rigidify the particles, but these particles undergo a buckling transition and gain an effective shape degree of freedom when their preferred perimeter is above a threshold value. We find that the mechanical response of jammed packings of deformable particles with shape degrees of freedom differs significantly from that of jammed packings of rigid particles even when they are compressed well above jamming onset, which emphasizes the importance of particle deformability in modelling soft solids.

Soft solids composed of deformable particles, such as foams [1, 2] and emulsions [3, 4], are ubiquitous in nature and industrial applications. Their mechanical and vibrational properties diverge from those of ideal elastic solids [5–8], in large part due to particle rearrangements and the ability of the particles to change their shape [9–11]. While extensive work over the past few decades has focused on *inter*particle interactions, less attention has been placed on how *intra*particle degrees of freedom affect collective behavior. In addition, many biological materials are composed of deformable objects, such microbiotic communities [12, 13], cell monolayers [14, 15], and tissues in both animals [16–23] and plants [24–28]. Shape degrees of freedom of individual particles influence material properties, but how single-particle deformability affects collective behavior remains largely unexplored.

We seek to investigate the mapping between single-particle properties and collective behavior by analyzing the harmonic vibrational response of jammed packings of deformable particles [29]. The vibrational response of jammed packings of spherical [30] and non-spherical [31–35] particles with rigid shapes has been used to determine the necessary conditions for system-spanning rigidity. For example, packings of N spherical particles in d spatial dimensions (with periodic boundary conditions) become mechanically stable with no non-trivial zero-frequency vibrational modes when they are isostatic [36, 37] and satisfy $dN - N_c = d - 1$, where N_c is the number of interparticle contacts. Jammed packings of non-spherical particles, however, are generically *hypo*static, with the number of degrees of freedom exceeding the number of interparticle contacts. These packings gain mechanical stability from higher-order terms ("quartic" modes) in the expansion of the potential energy, and the number of quartic modes matches the number of missing contacts [32]. Quartic modes have been observed in jammed packings of a variety of non-spherical particles [35, 38] and in jammed packings of "breathing" particles with size degrees of freedom [39].

Harmonic vibrational response can also be used to determine rigidity in vertex-based models of cellular materials. Previous work has identified a transition from floppy to rigid tissues, with the accompanying disappearance of non-trivial zero modes, as a function of the preferred cell perimeter [40–42]. While this work has demonstrated the importance of shape changes on bulk mechanical properties in soft solids, the vertex model mandates that cells are confluent and the use of vertex degrees of freedom (that are based on Voronoi tessellations) makes extracting single-cell mechanical properties from these models difficult. In this Letter, we will show how the shape degrees of freedom of individual particles contribute to bulk mechanical properties of soft solids using a computational model where each particle is distinct and explicitly deformable.

Systems of deformable particles in two dimensions are modeled by N distinct polygons, each with n_μ vertices with positions $\vec{r}_{i\mu}$ for $i = 1, ..., n_\mu$ and $\mu = 1, ..., N$. We

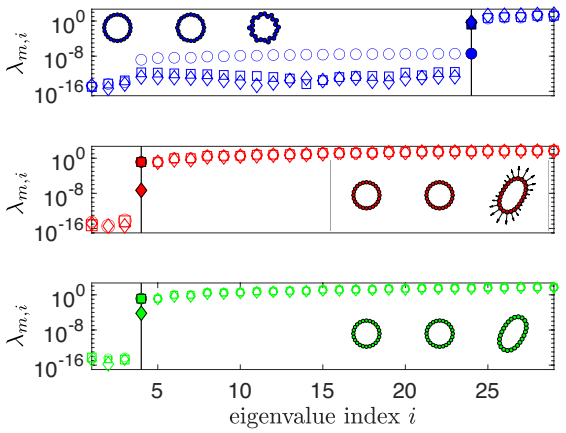

FIG. 1. **Single-particle vibrational response depends on shape energy.** In each row, we show the first 29 eigenvalues $\lambda_{m,i}$ of the dynamical matrix $\mathcal{M}$ for single particles with $n = 24$ vertices and three shape energies, DP, DPb, and DPbb, (Eqns. (1), (3), and (4) , with $U_{\rm int} = 0$) ordered from top to bottom. Insets show energy-minimized shapes for $\mathcal{A}_0/\mathcal{A}_n = 1$, 1.02, and 1.36 from left to right, and the corresponding eigenvalue spectra are plotted as circles, squares, and diamonds, respectively. Vertical lines are drawn at indices $i = 24$ in the top plot, and $i = 4$ in the middle and bottom plots. The associated eigenvalues are indicated by filled symbols. We draw representative curvature vectors $\vec{\kappa}_i$ from Eq. (3) along the perimeter of the third DPb particle in the second row. For the DPb and DPbb particles, we show λ_i for $K_b = 10^{-1}$ and $K_{bb} = 10^{-2}$.

use Greek indices to denote particle-based quantities, and Latin indices for vertex-based quantities. Each polygon has an area a_μ and perimeter $p_\mu = \sum_{i=1}^{n_\mu} l_{i\mu}$, where $l_{i\mu}$ is the edge joining vertex i and $i+1$ on polygon μ. In previous work [29], we studied the deformable polygon (DP) energy,

$$U = \frac{\epsilon_a}{2}\sum_{\mu=1}^{N}\left(\frac{a_\mu}{a_{0\mu}} - 1\right)^2 + \frac{\epsilon_l}{2}\sum_{\mu=1}^{N}\sum_{i=1}^{n_\mu}\left(\frac{l_{i\mu}}{l_{0\mu}} - 1\right)^2 + U_{\rm int}, \tag{1}$$

where $U_{\rm int}$ is the potential energy between interacting particles, and ϵ_a and ϵ_l are energies controlling area and perimeter fluctuations about the preferred area $a_{0\mu}$ and edge length $l_{0\mu}$, respectively. Interactions between vertices i and j on cells μ and ν are governed by the pair potential v, which we assume depends only on the distance between two vertices, $r_{ij}^{\mu\nu} = |\vec{r}_{i\mu} - \vec{r}_{j\nu}|$. We treat each vertex as a repulsive soft disk, where

$$v(r_{ij}^{\mu\nu}) = \frac{\epsilon_c}{2}\left(1 - \frac{r_{ij}^{\mu\nu}}{\sigma_{\mu\nu}}\right)^2 \Theta\left(1 - \frac{r_{ij}^{\mu\nu}}{\sigma_{\mu\nu}}\right), \tag{2}$$

$\sigma_{\mu\nu} = (l_{0\mu} + l_{0\nu})/2$, each vertex has diameter $l_{0\mu}$, ϵ_c controls the strength of the interaction, and Θ is the Heaviside step function to enforce purely repulsive interactions. The total interaction energy is therefore $U_{\rm int} = \sum_{\nu,\mu}\sum_{i=1}^{n_\mu}\sum_{j=1}^{n_\nu} v(r_{ij}^{\mu\nu})$, though we do not track overlaps between vertices i and $i+1$ and i and $i-1$ on the same cell. We measure lengths in units of the square root of the minimum preferred area, $\sqrt{a_0}$, energies in units of ϵ_a, and times in units of $\tau = \sqrt{a_0/\epsilon_a}$, where all vertex masses have been set to 1. The dimensionless *preferred* shape parameter $\mathcal{A}_{0\mu} = (n_\mu l_{0\mu})^2/(4\pi a_{0\mu})$ measures the amount of excess perimeter above a regular polygon with area $a_{0\mu}$ and thus $\mathcal{A}_{0\mu}$ controls particle deformability [29]. For the DP model, particle shapes depend only on $K_l = \epsilon_l/\epsilon_a$, $K_c = \epsilon_c/\epsilon_a$, and $\mathcal{A}_{0\mu}$.

We first investigate the rigidity of single DP particles by analyzing the eigenvalues $\lambda_{m,i}$ of the dynamical matrix $\mathcal{M}_{kl} = \partial^2 U/\partial\vec{r}_k\partial\vec{r}_l$. We find the energy-minimized shapes of single particles using the FIRE algorithm [43]. In Fig. 1, we plot the first 29 eigenvalues $\lambda_{m,i}$ for particles with $n = 24$ vertices, $K_l = 1$, and $\mathcal{A}_0/\mathcal{A}_n = 1$, 1.02, and 1.36, where $\mathcal{A}_n = n\tan(\pi/n)/\pi$ is the shape parameter for a regular polygon with n vertices. Using constraint counting, DP particles with $2n$ degrees of freedom, n perimeter constraints, one area constraint, and 3 trivial zero modes (two translations and one rotation) should have $2n - (n+1) - 3 = n - 4$ unconstrained shape degrees of freedom [37, 44]. In Fig. 1, we show that DP particles possess $n-4$ eigenvalues $\lambda_{m,i}$ of similarly small magnitudes ($\sim 10^{-15} - 10^{-14}$) to the 3 trivial zero modes. However, we also show in Fig. 1 that DP particles with $\mathcal{A}_0 = \mathcal{A}_n$ have $n-3$ low-frequency modes ($\lambda_{m,i} \sim 10^{-8}$, blue circles in Fig. 1) that are significantly larger than the apparent zero modes when $\mathcal{A}_0 > \mathcal{A}_n$. These low-frequency modes are stabilized by the geometric constraint that regular polygons minimize the perimeter-to-area ratio; deviations from this shape will cost energy even though the vertices are underconstrained. Thus, setting $\mathcal{A}_0 < \mathcal{A}_n$ generates stress in the area and perimeter contributions to the DP energy, which stabilizes the $n-4$ shape degrees of freedom. Many deformable particles are incompressible, therefore we will restrict our analysis to the case $\mathcal{A}_0 \geq \mathcal{A}_n$ to avoid fluctuations in the particle area.

To rigidify single DP particles, we add n additional bending constraints along the particles' perimeters [29],

$$U_b = \frac{k_b}{2}\sum_{i=1}^{n}\vec{\kappa}_i^2, \qquad \vec{\kappa}_i = \frac{\vec{l}_i - \vec{l}_{i-1}}{l_0^2}. \tag{3}$$

where k_b is the bending modulus, and we refer to particles with this additional energy term as DPb particles. This bending energy is similar to those used in models of semiflexible polymers [45]. In the second row of Fig. 1, we show the first 29 eigenvalues for DPb particles with $n = 24$ vertices, as well as representative energy-minimized shapes for $K_b = k_b/(\epsilon_a l_0^2) = 10^{-1}$. We also introduce an additional constraint on the average distance between

opposite vertices (a "belt" spring), which gives the DPbb model,

$$U_{bb} = \frac{\epsilon_{bb}}{2}\left(\frac{\overline{D}}{D_0} - 1\right)^2, \qquad \overline{D} = \frac{2}{n}\sum_{i=1}^{n/2}\left|\vec{r}_{i+n/2} - \vec{r}_i\right|, \quad (4)$$

where $D_0 = l_0/\sin(\pi/n)$ is the distance between opposing vertices of a regular n-sided polygon with edge length l_0. We show representative eigenvalues $\lambda_{m,i}$ and energy-minimized shapes in the third row of Fig. 1 for $K_{bb} = \epsilon_{bb}/\epsilon_a = 10^{-2}$. The additional n or $n+1$ constraints in the DPb or DPbb models constrain the particle shape to a regular polygon when $\mathcal{A}_0 \simeq \mathcal{A}_n$, as the particle shapes are now *over*constrained compared to DP particles. However, as shown in the second row of Fig. 1 (red diamonds), DPb particles "buckle" when the preferred shape parameter $\mathcal{A}_0$ exceeds a threshold $\mathcal{A}_0^*$, and the first non-trivial eigenvalue $\lambda_{m,4}$ becomes small. In the Supplementary Material (SM) [46], we show that an alternative bending energy with next-to-nearest neighbor (NNN) perimeter springs, which have been shown to rigidify undercoordinated lattices [47], has qualitatively similar buckling behavior, where the first non-trivial eigenvalue $\lambda_{m,4} \to 0$ at the buckling transition. Note that DPbb particles (Fig. 1, green diamonds) also buckle above a characteristic shape parameter, but $\lambda_{m,4}$ remains comparable in magnitude to the other non-trivial eigenvalues.

To investigate how single-particle deformability influences collective behavior, we prepare jammed packings of N bidisperse (50:50 by number) deformable particles in square cells with side length L and periodic boundary conditions. Small (large) particles are given $n_\mu = 16$ (22) vertices, and the segment lengths $l_{0\mu}$ are chosen such that $\mathcal{A}_{0\mu}/\mathcal{A}_n$ is identical for each particle. Large particles are given preferred areas $a_{0\mu} = (22/16)^2\overline{a}_0$. As in Ref. [29], particles are first placed randomly in the simulation cell at low packing fraction ϕ. We then isotropically compress the system in small packing fraction increments $\Delta\phi$, with each compression step followed by minimization of the total potential energy U using FIRE, until the system finds a force- and torque-balanced configuration with total root-mean-square force, $F_{\rm rms} = \sqrt{N^{-1}\sum_\mu n_\mu^{-1}\sum_i (\boldsymbol{\nabla}_{i\mu}U)^2} < 10^{-12}$ and minimal interparticle overlaps. We monitor jamming onset using the virial pressure $P = (\Sigma_{xx}+\Sigma_{yy})/2$, where the virial stress is

$$\Sigma_{\xi\xi'} = \epsilon_c L^{-2}\sum_{\nu\neq\mu}\sum_{i=1}^{n_\mu}\sum_{j=1}^{n_\nu}\left(1 - \frac{r_{ij}^{\mu\nu}}{\sigma_{ij}^{\mu\nu}}\right)\frac{r_{ij,\xi}^{\mu\nu}r_{ij,\xi'}^{\mu\nu}}{r_{ij}^{\mu\nu}\sigma_{ij}^{\mu\nu}}. \quad (5)$$

$r_{ij,\xi}^{\mu\nu}$ is the ξ-component of the vector separating vertex i on cell μ and vertex j on cell ν and $\xi = x$ or y. We identify jamming onset, with packing fraction ϕ_J, when the pressure $10^{-7} < P < 2\times10^7$. We have confirmed that the results do not depend on the pressure threshold as long as it is sufficiently small.

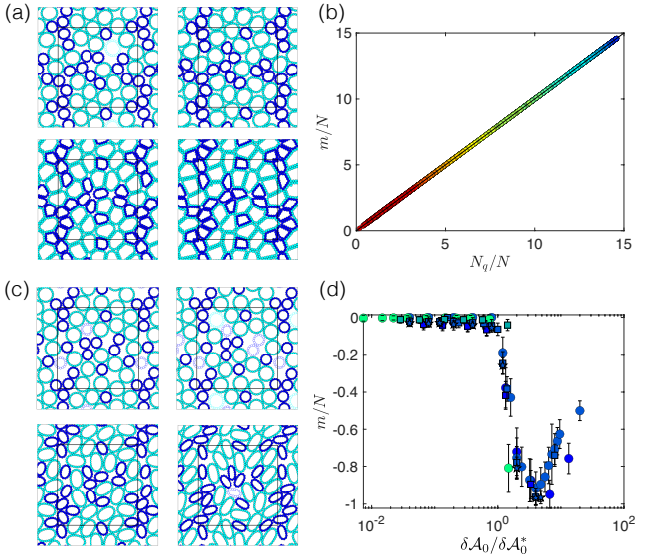

FIG. 2. **DP packings are hypostatic, DPb packings are hyperstatic.** (a) Four representative jammed packings of $N = 32$ bidisperse DP particles with $\mathcal{A}_0/\mathcal{A}_n = 1.001$, 1.02, 1.1, and 1.2. Vertices on particles with zero vertex-vertex contacts are drawn with open circles. (b) Number of missing contacts per particle m/N in packings of $N = 32$ DP particles vs. number of quartic modes per particle N_q/N. Black solid line gives $m = N_q$, and colors represent shape parameter values from $\mathcal{A}_0/\mathcal{A}_n = 1.0001$ to 1.24, sorted from low (blue) to high (red) values. (c) Same as (a), but for $N = 32$ DPb particles with $K_b = 10^{-2}$. (d) m/N in packings of DPb particles plotted vs. $\delta\mathcal{A}_0/\delta\mathcal{A}_0^* = (\mathcal{A}_0 - \mathcal{A}_n)/(\mathcal{A}_0^* - \mathcal{A}_n)$, where $\mathcal{A}_0^*$ is the buckling shape parameter. Colors represent K_b (sorted from blue to green), spanning $K_b = 0.005$ to 0.05, and shapes represent different system sizes: $N = 16$ (circles), 32 (squares), and 64 (stars).

Example packings of DP and DPb particles are shown in Fig. 2 (a) and (c). In Fig. 2 (a), DP particles with larger $\mathcal{A}_0$ jam at increasingly higher packing fractions due to increased particle deformability [29], while in Fig. 2 (c), jammed packings of DPb particles resemble packings of rigid "bumpy" disks [34], dimers [35, 48] and ellipses [29], depending on the preferred shape parameter of the particles. While jamming onset for DP particles occurs at large packing fractions when the particles are more deformable, we show in Fig. 2 (b) these packings are *hypo*static with fewer contacts than expected from constraint counting.

As described above, each DP particle has $n_\mu + 1$ internal shape constraints, so a packing with $N_{\rm vv}$ vertex-vertex contacts gives a total of $N(\overline{n}+1) + N_{\rm vv}$ constraints, where $\overline{n} = N^{-1}\sum_\mu n_\mu$ is the mean number of vertices per particle. An isostatic packing would then have $N_{\rm vv}^{\rm iso} = N(\overline{n}-1) - 1$ contacts. However, we show in Fig. 2 (b) that the number of *missing* contacts

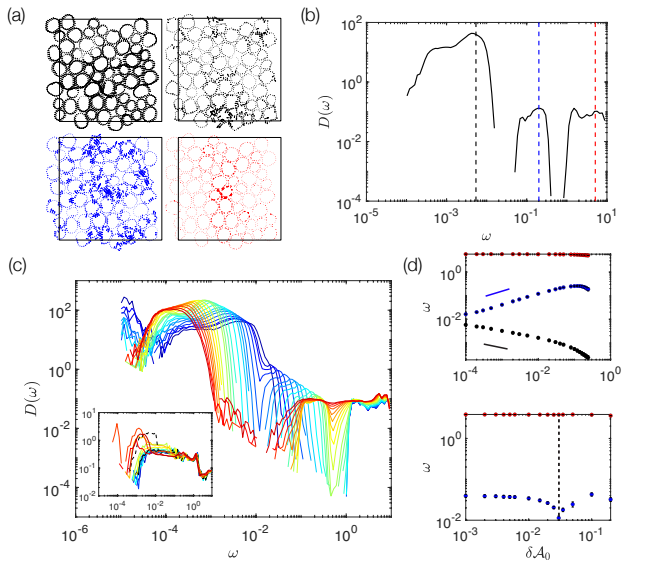

FIG. 3. **Quartic modes and buckling strongly influence low-frequency behavior of vibrational response.** (a) Visualization of representative eigenmodes in a jammed packing of $N = 64$ DP particles with $\mathcal{A}_0/\mathcal{A}_n = 1.02$. Top-left and -right are quartic modes at low frequency and near ω_0, respectively, while bottom-left and -right are typical modes in the mid- and high-frequency bands near ω_1 and ω_2, respectively. (b) Density of vibrational modes $D(\omega)$ for the same system in (a). Vertical lines are drawn at ω_0, ω_1, and ω_2. (c) $D(\omega)$ for jammed packings of $N = 32$ DP particles (inset is DPb with $K_b = 10^{-2}$). Color represents $\mathcal{A}_0/\mathcal{A}_n$ from 1.0001 to 1.24 sorted from blue to red. The black solid and dashed lines in the inset indicate $D(\omega)$ for DPb packings with $\mathcal{A}_0/\mathcal{A}_n = 1.01$ and 1.03, which are respectively below and at the buckling transition $\mathcal{A}_0^*$. (d) Characteristic frequencies ω_0 (black), ω_1 (blue), and ω_2 (red) as a function of $\delta\mathcal{A}_0 = (\mathcal{A}_0 - \mathcal{A}_n)/\mathcal{A}_n$ for DP (top) and DPb (bottom) packings. In the top panel, black and blue lines represent $\omega \sim \delta\mathcal{A}_0^{-1/3}$ and $\sim \delta\mathcal{A}_0^{1/2}$, respectively. In the bottom panel, the vertical dashed line corresponds to $\delta\mathcal{A}_0^*$.

$m = N_{\rm vv}^{\rm iso} - N_{\rm vv} > 0$ for DP packings at jamming onset. Hypostatic jammed packings are ubiquitous in systems with non-spherical particles [39], and recent work has shown that the extra degrees of freedom can be stabilized by higher-order "quartic" modes of the potential energy [32, 35]. In the SM [46], we show that quartic modes can be identified by decomposing the dynamical matrix $\mathcal{M}$ into stiffness $\mathcal{H}$ and stress $\mathcal{S}$ matrices [31, 49]. We show in Fig. 2 (b) that the number of missing contacts is exactly matched by the number of quartic modes N_q in each DP packing.

DPb particles, however, can form *hyper*static packings at jamming onset, where the number of interparticle contacts exceeds the minimal number required to constrain the particle degrees of freedom. In Fig. 2 (d), we show that $m \sim 0$ when the preferred shape parameter $\mathcal{A}_0 < \mathcal{A}_0^*$. Here, $m = N_{\rm vv}^{\rm iso} - N_{\rm vv}$, but the DPb single-particle energy is overconstrained, so DPb particles have 3 degrees of freedom each and $N_{\rm vv}^{\rm iso} = 3N - 1$. However, $m < 0$ when jammed packings are generated with buckled DPb particles. This surprising result is likely due to buckling of single DPb particles (Fig. 1), which is signaled by the rapid decrease of $\lambda_{m,4}$. When particles are buckled and $0 < \lambda_{m,4} \ll 1$, transiently isostatic, but ultimately unstable networks of interparticle contacts are formed and broken due to low-frequency shape changes along the $\lambda_{m,4}$-eigenvector. We verify this behavior by showing in the SM [46] that a single buckled DPb particle has an ultra-low frequency shape mode when pinned by two fixed vertices, even though the DPb particle has four contacts and would be iso-constrained if it were rigid. We decompose vibrational eigenmodes into translational (T), rotational (R), and shape (S) components in the SM [46], and show that DPb packings always have a non-zero contribution of S at low-frequencies when we take the rigid-particle limit $K_c \to 0$. However, $S \to 0$ for the first $3N$ modes in packings of DPbb particles when we take the rigid-particle limit, suggesting that the addition of the "belt" spring fully rigidifies the particle shape.

To further investigate the collective behavior, we compute the density of vibrational modes $D(\omega)$ for modes with frequency $\omega_i = \sqrt{\lambda_{m,i}}$. We find that $D(\omega)$ varies dramatically across each model of single-particle deformability. In packings of DP particles, we observe three distinct bands of vibrational response in Fig. 3 (a)-(f) due to quartic modes (with mean frequency ω_0), mid-frequency collective modes (with mean frequency ω_1), and high-frequency shape modes (with mean frequency

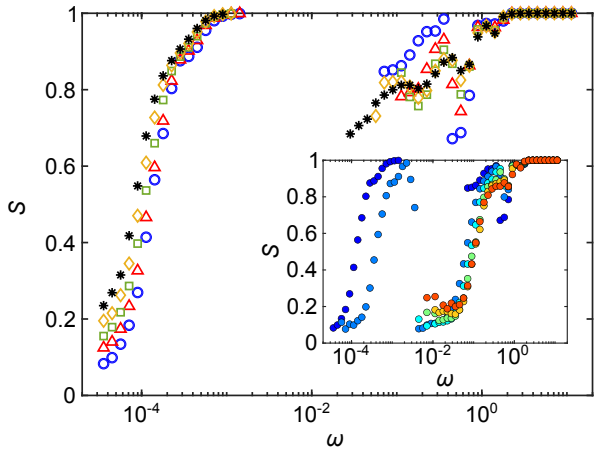

FIG. 4. **Shape degrees of freedom account for a significant fraction of vibrational response in DP packings.** Magnitude of mode projection onto the shape degrees of freedom (S) versus eigenmode frequency ω for DP packings with $N = 256$ and $\mathcal{A}_0/\mathcal{A}_n = 1.02$ (circles), 1.06 (triangles), 1.1 (squares), 1.14 (diamonds), and 1.18 (asterisks). Inset: $S(\omega)$ for DP packings with $\mathcal{A}_0/\mathcal{A}_n = 1.02$ at several packing fractions from $\phi = \phi_J$ (blue circles) to 0.98 (red circles) in ϕ increments of 2×10^{-2}.

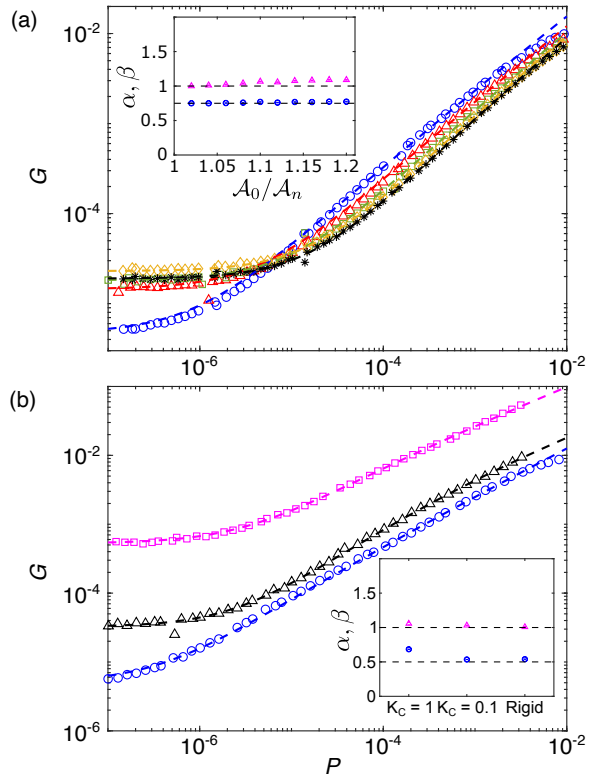

FIG. 5. **Shear response differs in particle models with increasing deformability.** (a) Static shear modulus G versus pressure P for $N = 256$ DP packings with $\mathcal{A}_0/\mathcal{A}_n = 1.02$ (circles), 1.06 (triangles), 1.1 (squares), 1.14 (diamonds), and 1.18 (asterisks). The dashed lines are best fits to Eq. 6. Inset: Exponents α (triangles) and β (circles) from Eq. 6 for data in (a) versus $\mathcal{A}_0$. Horizontal lines indicate $\alpha = 1.0$ and $\beta = 0.75$. (b) $G(P)$ for $N = 128$ DPbb packings with $\mathcal{A}_0/\mathcal{A}_n = 1.02$ for $K_c = 1$ (circles) and 10^{-1} (triangles) and rigid, bumpy ellipses with the same shape parameter (squares). All DPbb systems have $K_l = 1$, $K_b = 10^{-1}$ and $K_{bb} = 10^{-2}$. The dashed lines are best fits to Eq. 6. Inset: Exponents α (triangles) and β (circles) from Eq. 6 for models with increasing rigidity. Horizontal lines indicate $\alpha = 1.0$ and $\beta = 0.5$.

ω_2). In the SM [46], we show that $D(\omega)$ and the characteristic frequencies do not change significantly with system size. A similar three-band structure is found in the vibrational response of jammed packings of rigid non-spherical particles [35], although here the second band of modes corresponds to shape fluctuations at particle-particle interfaces rather than particle rotations. Additionally, in Fig. 3 (g), we find a characteristic scaling $\omega_0 \sim \delta\mathcal{A}_0^{-1/3}$, indicating collective motion becomes less costly as particles become more deformable. This result differs from that for frictionless non-spherical particles with rigid shape [39, 49], where the exponent $\sim 1/2$ for the scaling of ω_0 with shape parameter. We find approximate 1/2 scaling with shape parameter in the mid-frequency band ω_1, although this exponent is ~ 1 in packings of rigid non-spherical particles. The stiff shape mode band with mean frequency ω_2 does not vary with particle shape, as these modes are controlled solely by the perimeter spring constant K_l and not on interparticle contacts. We also computed $D(\omega)$ for packings of DPb particles, as shown in Fig. 3 (h). Since there are no quartic modes in DPb packings, there is no ω_0 band. Also, we do not observe distinct band structure separating ω_1 and ω_2. The only role shape plays in the vibrational response for DPb particles is that there is a cusp in ω_1 near $\mathcal{A}_0^*$ (inset to Fig. 3 (h)), and an increased density of vibrational modes at lower frequencies. This observation is consistent with the inability of the DPb model to reach the rigid-particle limit (see SM [46]), and is likely due to the small value of $\lambda_{m,4}$ in buckled DPb particles.

We find that the shape degrees of freedom always play an important role in the collective response for DP packings. In Fig. 4, we show that low-frequency modes have a significant shape contribution $S(\omega)$ in DP packings with preferred shape parameters $1.02 \leq \mathcal{A}_0/\mathcal{A}_n \leq 1.18$. We find that $S(\omega)$ remains > 0 even as ω_0 grows with increasing compression. Previous studies of driven amorphous solids have argued that deformability can be captured by spherical particles with soft interparticle potentials [9]. Here, we find that, for sufficiently deformable particles, explicit shape change accounts for a large fraction of the total vibrational response. Explicit shape change is therefore necessary to capture important features of driven soft materials, such as flows of bubbles [2] and emulsions [50, 51].

To investigate the effect of particle deformability on bulk mechanical properties, we computed the static shear modulus G for jammed packings of DP and DPbb particles. Packings were compressed to a given pressure P, subjected to small, successive simple shear steps of size $\Delta\gamma$ with Lees-Edwards boundary conditions [52], and energy-minimized after each step. We measure $G = -\partial\Sigma_{xy}/\partial\gamma$, where Σ_{xy} is the virial shear stress. We report G averaged over an ensemble of at least 500 configurations. In Fig. 5, we show that, although DP packings contains collective low-frequency quartic modes, they possess $G > 0$ at low pressure [29, 32]. In the SM [46], we also show characteristic N^{-1} scaling of G in the $P \to 0$ limit [53]. We find in Fig. 5 (a) that $G(P)$ for DP packings over of wide range of $\mathcal{A}_0$ is well-approximated by a double-power-law functional form [54] used to describe the shear response of packings of soft frictionless spheres:

$$G = G_0 + \frac{aP^\alpha}{1 + cP^{\alpha-\beta}} \tag{6}$$

Values of $\alpha \approx 1$ and $\beta \approx 0.5$ have been reported in previous studies of jammed packings of frictionless spherical particles [6, 53], frictional spherical particles [55], and bumpy particles [34]. However, we find that the large pressure scaling exponent $\beta \approx 0.75$ for DP packings. In Fig. 5 (b), we show that we recover the $\beta \approx 0.5$ scaling

exponent by taking the rigid-particle limit (DPbb particles and $K_c \to 0$) and for rigid, bumpy ellipse-shaped particles with identical $\mathcal{A}_0/\mathcal{A}_n$. For packings of less-rigid DPbb particles, we obtain $\beta \approx 0.6$, suggesting that DPbb particles away from the rigid-particle limit possess bulk mechanical properties between those of truly deformable, DP particles and those of truly rigid particles with no shape degrees of freedom.

This work has demonstrated that truly deformable particles with explicit shape degrees of freedom can form amorphous jammed solids, but that their vibrational and mechanical response differs significantly from jammed packings of particles without shape degrees of freedom. In particular, the scalings $\omega_0 \sim \delta\mathcal{A}_0^{-1/3}$ and $G \sim P^{3/4}$ observed for jammed DP packings indicate important differences from previous studies of jammed packings of soft particles without shape degrees of freedom [6, 39, 53]. In future work, we will investigate why hyperstatic packings occur for buckled DPb particles at jamming onset by developing a theoretical framework that determines exactly the number of degrees of freedom for each particle near jamming onset. Here, we focused on linear response, but in future studies, we will also consider driven, soft solids [50, 51] and motile tissues [56] to uncover how explicit particle deformability impacts transport and diffusion both close to and far from the jamming transition.

We acknowledge support from NSF Grants No. CBET-2002782 (J.T. and C.O.), No. CBET-2002797 (M.S.), and No. CMMI-1463455 (M.S.) and NIH award No. 5U54CA210184-04 (D.W.). This work was also supported by the High Performance Computing facilities operated by Yale's Center for Research Computing.

* These authors contributed equally.
† corey.ohern@yale.edu

[1] F. Bolton and D. Weaire, Rigidity loss transition in a disordered 2d froth, Phys. Rev. Lett. **65**, 3449 (1990).
[2] Y. Bertho, C. Becco, and N. Vandewalle, Dense bubble flow in a silo: An unusual flow of a dispersed medium, Phys. Rev. E **73**, 056309 (2006).
[3] H. Princen, Rheology of foams and highly concentrated emulsions: I. elastic properties and yield stress of a cylindrical model system, J. Colloid. Interf Sci. **91**, 160 (1983).
[4] A. Boromand, A. Signoriello, J. Lowensohn, C. S. Orellana, E. R. Weeks, F. Ye, M. D. Shattuck, and C. S. O'Hern, The role of deformability in determining the structural and mechanical properties of bubbles and emulsions, Soft Matter **15**, 5854 (2019).
[5] M. L. Falk and J. S. Langer, Dynamics of viscoplastic deformation in amorphous solids, Phys. Rev. E **57**, 7192 (1998).
[6] C. S. O'Hern, L. E. Silbert, A. J. Liu, and S. R. Nagel, Jamming at zero temperature and zero applied stress: The epitome of disorder, Phys. Rev. E **68**, 011306 (2003).
[7] C. P. Goodrich, A. J. Liu, and S. R. Nagel, Solids between the mechanical extremes of order and disorder, Nat. Phys. **10**, 578 (2014).
[8] D. Bonn, M. M. Denn, L. Berthier, T. Divoux, and S. Manneville, Yield stress materials in soft condensed matter, Rev. Mod. Phys. **89**, 035005 (2017).
[9] D. J. Durian, Foam mechanics at the bubble scale, Phys. Rev. Lett. **75**, 4780 (1995).
[10] M. van Hecke, Jamming of soft particles: geometry, mechanics, scaling and isostaticity, J. Phys.: Condens. Matter **22**, 033101 (2009).
[11] C. F. Schreck, T. Bertrand, C. S. O'Hern, and M. D. Shattuck, Repulsive contact interactions make jammed particulate systems inherently nonharmonic, Phys. Rev. Lett. **107**, 078301 (2011).
[12] W. P. J. Smith, Y. Davit, J. M. Osborne, W. Kim, K. R. Foster, and J. M. Pitt-Francis, Cell morphology drives spatial patterning in microbial communities, Proc. Natl. Acad. Sci. USA **114**, E280 (2017).
[13] F. Beroz, J. Yan, Y. Meir, B. Sabass, H. A. Stone, B. L. Bassler, and N. S. Wingreen, Verticalization of bacterial biofilms, Nat. Phys. **14**, 954 (2018).
[14] J.-A. Park, J. H. Kim, D. Bi, J. A. Mitchel, N. T. Qazvini, K. Tantisira, C. Y. Park, M. McGill, S.-H. Kim, B. Gweon, J. Notbohm, R. Steward Jr, S. Burger, S. H. Randell, A. T. Kho, D. T. Tambe, C. Hardin, S. A. Shore, E. Israel, D. A. Weitz, D. J. Tschumperlin, E. P. Henske, S. T. Weiss, M. L. Manning, J. P. Butler, J. M. Drazen, and J. J. Fredberg, Unjamming and cell shape in the asthmatic airway epithelium, Nat. Mater. **14**, 1040 (2015).
[15] X. Trepat and E. Sahai, Mesoscale physical principles of collective cell organization, Nat. Phys. **14**, 671 (2018).
[16] T. Lecuit and P.-F. Lenne, Cell surface mechanics and the control of cell shape, tissue patterns and morphogenesis, Nat. Rev. Mol. Cell Bio. **8**, 633 (2007).
[17] M. Murrell, P. W. Oakes, M. Lenz, and M. L. Gardel, Forcing cells into shape: the mechanics of actomyosin contractility, Nat. Rev. Mol. Cell Bio. **16**, 486 (2015).
[18] M. K. Jolly, M. Boareto, B. Huang, D. Jia, M. Lu, E. Ben-Jacob, J. N. Onuchic, and H. Levine, Implications of the hybrid epithelial/mesenchymal phenotype in metastasis, Front. Oncol. **5**, 155 (2015).
[19] P. McMillen, V. Chatti, D. Jülich, and S. A. Holley, A sawtooth pattern of cadherin 2 stability mechanically regulates somite morphogenesis, Curr. Biol. **26**, 542 (2016).
[20] L. Oswald, S. Grosser, D. M. Smith, and J. A. Käs, Jamming transitions in cancer, J. Phys. D Appl. Phys. **50**, 483001 (2017).
[21] A. Mongera, P. Rowghanian, H. J. Gustafson, E. Shelton, D. A. Kealhofer, E. K. Carn, F. Serwane, A. A. Lucio, J. Giammona, and O. Campàs, A fluid-to-solid jamming transition underlies vertebrate body axis elongation, Nature **561**, 401 (2018).
[22] O. Ilina, P. G. Gritsenko, S. Syga, J. Lippoldt, C. A. M. La Porta, O. Chepizhko, S. Grosser, M. Vullings, G.-J. Bakker, J. Starruß, P. Bult, S. Zapperi, J. A. Käs, A. Deutsch, and P. Friedl, Cell–cell adhesion and 3d matrix confinement determine jamming transitions in breast cancer invasion, Nat. Cell Biol. **22**, 1103 (2020).
[23] S. Kim, M. Pochitaloff, G. A. Stooke-Vaughan, and O. Campàs, Embryonic tissues as active foams, bioRxiv 10.1101/2020.06.17.157909 (2020).
[24] N. Wuyts, J.-C. Palauqui, G. Conejero, J.-L. Verdeil, C. Granier, and C. Massonnet, High-contrast three-

dimensional imaging of the arabidopsis leaf enables the analysis of cell dimensions in the epidermis and mesophyll, Plant Methods **6**, 17 (2010).
[25] S. Kalve, J. Fotschki, T. Beeckman, K. Vissenberg, and G. T. S. Beemster, Three-dimensional patterns of cell division and expansion throughout the development of Arabidopsis thaliana leaves, J. Exp. Bot. **65**, 6385 (2014).
[26] A. Sapala, A. Runions, A.-L. Routier-Kierzkowska, M. Das Gupta, L. Hong, H. Hofhuis, S. Verger, G. Mosca, C.-B. Li, A. Hay, O. Hamant, A. H. Roeder, M. Tsiantis, P. Prusinkiewicz, and R. S. Smith, Why plants make puzzle cells, and how their shape emerges, eLife **7**, e32794 (2018).
[27] P. Martinez, L. A. Allsman, K. A. Brakke, C. Hoyt, J. Hayes, H. Liang, W. Neher, Y. Rui, A. M. Roberts, A. Moradifam, B. Goldstein, C. T. Anderson, and C. G. Rasmussen, Predicting division planes of three-dimensional cells by soap-film minimization, Plant Cell **30**, 2255 (2018).
[28] A. M. Borsuk, A. B. Roddy, G. Théroux-Rancourt, and C. R. Brodersen, Emergent honeycomb topology of the leaf spongy mesophyll, bioRxiv 10.1101/852459 (2019).
[29] A. Boromand, A. Signoriello, F. Ye, C. S. O'Hern, and M. D. Shattuck, Jamming of deformable polygons, Phys. Rev. Lett. **121**, 248003 (2018).
[30] M. Wyart, S. R. Nagel, and T. A. Witten, Geometric origin of excess low-frequency vibrational modes in weakly connected amorphous solids, Europhys. Lett. **72**, 486 (2005).
[31] A. Donev, R. Connelly, F. H. Stillinger, and S. Torquato, Underconstrained jammed packings of nonspherical hard particles: Ellipses and ellipsoids, Phys. Rev. E **75**, 051304 (2007).
[32] M. Mailman, C. F. Schreck, C. S. O'Hern, and B. Chakraborty, Jamming in systems composed of frictionless ellipse-shaped particles, Phys. Rev. Lett. **102**, 255501 (2009).
[33] Z. Zeravcic, N. Xu, A. J. Liu, S. R. Nagel, and W. van Saarloos, Excitations of ellipsoid packings near jamming, Europhys. Lett. **87**, 26001 (2009).
[34] S. Papanikolaou, C. S. O'Hern, and M. D. Shattuck, Isostaticity at frictional jamming, Phys. Rev. Lett. **110**, 198002 (2013).
[35] K. VanderWerf, W. Jin, M. D. Shattuck, and C. S. O'Hern, Hypostatic jammed packings of frictionless nonspherical particles, Phys. Rev. E **97**, 012909 (2018).
[36] A. V. Tkachenko and T. A. Witten, Stress propagation through frictionless granular material, Phys. Rev. E **60**, 687 (1999).
[37] T. C. Lubensky, C. L. Kane, X. Mao, A. Souslov, and K. Sun, Corrigendum: Phonons and elasticity in critically coordinated lattices, Rep. Prog. Phys. **78**, 109501 (2015).
[38] Y. Yuan, K. VanderWerf, M. D. Shattuck, and C. S. O'Hern, Jammed packings of 3d superellipsoids with tunable packing fraction, coordination number, and ordering, Soft Matter **15**, 9751 (2019).
[39] C. Brito, H. Ikeda, P. Urbani, M. Wyart, and F. Zamponi, Universality of jamming of nonspherical particles, Proc. Natl. Acad. Sci. USA **115**, 11736 (2018).
[40] D. Bi, J. H. Lopez, J. M. Schwarz, and M. L. Manning, A density-independent rigidity transition in biological tissues, Nat. Phys. **11**, 1074 (2015).
[41] M. Merkel and M. L. Manning, A geometrically controlled rigidity transition in a model for confluent 3d tissues, New J. Phys. **20**, 022002 (2018).
[42] L. Yan and D. Bi, Multicellular rosettes drive fluid-solid transition in epithelial tissues, Phys. Rev. X **9**, 011029 (2019).
[43] E. Bitzek, P. Koskinen, F. Gähler, M. Moseler, and P. Gumbsch, Structural relaxation made simple, Phys. Rev. Lett. **97**, 170201 (2006).
[44] S. Pellegrino, Structural computations with the singular value decomposition of the equilibrium matrix, Int. J. Solids Struct. **30**, 3025 (1993).
[45] S. M. Rappaport and Y. Rabin, Bending affects entropy of semiflexible polymers: Application to protein-dna complexes, Phys. Rev. E **80**, 052801 (2009).
[46] Supplementary information url.
[47] X. Mao, N. Xu, and T. C. Lubensky, Soft modes and elasticity of nearly isostatic lattices: Randomness and dissipation, Phys. Rev. Lett. **104**, 085504 (2010).
[48] C. F. Schreck, N. Xu, and C. S. O'Hern, A comparison of jamming behavior in systems composed of dimer- and ellipse-shaped particles, Soft Matter **6**, 2960 (2010).
[49] C. F. Schreck, M. Mailman, B. Chakraborty, and C. S. O'Hern, Constraints and vibrations in static packings of ellipsoidal particles, Phys. Rev. E **85**, 061305 (2012).
[50] X. Hong, M. Kohne, M. Morrell, H. Wang, and E. R. Weeks, Clogging of soft particles in two-dimensional hoppers, Phys. Rev. E **96**, 062605 (2017).
[51] I. Golovkova, L. Montel, E. Wandersman, T. Bertrand, A. M. Prevost, and L.-L. Pontani, Depletion attraction impairs the plasticity of emulsions flowing in a constriction, Soft Matter **16**, 3294 (2020).
[52] M. P. Allen and D. J. Tildesley, *Computer Simulation of Liquids*, 2nd ed. (Oxford University Press, 2017).
[53] C. P. Goodrich, A. J. Liu, and S. R. Nagel, Finite-size scaling at the jamming transition, Phys. Rev. Lett. **109**, 095704 (2012).
[54] K. VanderWerf, A. Boromand, M. D. Shattuck, and C. S. O'Hern, Pressure dependent shear response of jammed packings of frictionless spherical particles, Phys. Rev. Lett. **124**, 038004 (2020).
[55] E. Somfai, M. van Hecke, W. G. Ellenbroek, K. Shundyak, and W. van Saarloos, Critical and noncritical jamming of frictional grains, Phys. Rev. E **75**, 020301(R) (2007).
[56] V. Ajeti, A. P. Tabatabai, A. J. Fleszar, M. F. Staddon, D. S. Seara, C. Suarez, M. S. Yousafzai, D. Bi, D. R. Kovar, S. Banerjee, and M. P. Murrell, Wound healing coordinates actin architectures to regulate mechanical work, Nat. Phys. **15**, 696 (2019).